ACS OMEGA

Open Access

http://pubs.acs.org/journal/acsodf

Article

Understanding the Interaction Mechanism between the Epinephrine Neurotransmitter and Small Gold Nanoclusters (Au_n; n = 6, 8, and 10): A Computational Insight

Nagendra Prasad Yadav,* Tarun Yadav, Sangram Pattanaik, Ehsan Shakerzadeh, Subhendu Chakroborty,* Cai Xiaofeng, Anil Kumar Vishwkarma,* Amit Pathak, Jitendra Malviya, and Fanindra Pati Pandey

Cite This: *ACS Omega* 2024, 9, 3373−3383

Read Online

ACCESS | Metrics & More | Article Recommendations | Supporting Information

ABSTRACT: In this study, the interaction between the neurotransmitter epinephrine and small gold nanoclusters (Au_nNCs) with n = 6, 8, and 10 is described by density functional theory calculations. The interaction of Au_6, Au_8, and Au_{10} nanoclusters with epinephrine is governed by Au-X (X = N and O) anchoring bonding and Au···H-X conventional hydrogen bonding. The interaction mechanism of epinephrine with gold nanoclusters is investigated in terms of electronic energy and geometrical properties. The adsorption energy values for the most favorable configurations of Au_6NC@epinephrine, Au_8NC@epinephrine, and Au_{10}NC@epinephrine were calculated to be −17.45, −17.86, and −16.07 kcal/mol, respectively, in the gas phase. The results indicate a significant interaction of epinephrine with Au_nNCs and point to the application of the biomolecular complex Au_nNC@epinephrine in the fields of biosensing, drug delivery, bioimaging, and other applications. In addition, some important electronic properties, namely, the energy gap between HOMO and LUMO, the Fermi level, and the work function, were computed. The effect of aqueous media on adsorption energy and electronic parameters for the most favorable configurations was also studied to explore the influence of physical biological conditions.

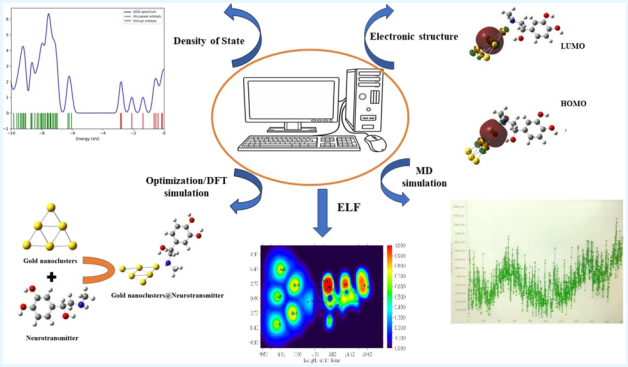

1. INTRODUCTION

Nanomaterials such as nanoparticles (NPs) or nanoclusters (NCs) have shown considerable potential for a range of biomedical and industrial applications including medication administration, plasmonics, chemical sensors, photonics, antimicrobial activities, cell electrodes, antimicrobial coating, optical devices, hyperthermia therapy, and diagnostics.[1−8] Therefore, a detailed understanding of the binding or adsorption mechanism of biomolecules with NPs and NCs is a very important task. There are a number of theoretical and experimental studies on the adsorption behavior of different types of nanomaterials, namely, silver nanoparticles, gold nanoparticles (AuNPs), carbon nanotubes, fullerenes with nucleic acids, biomolecules, proteins, peptides, and neurotransmitters, to explore their efficacy for drug delivery and biosensor applications.[9−17] Among the various available inorganic nanomaterials, AuNPs/gold nanoclusters (AuNCs) have been attracted substantial research due to their distinctive characteristics, which make them appropriate for a variety of applications in diverse sectors such as biomedicine, detection of cancer cells, wound healing, electronics, targeted drug delivery, and catalysis.[18−22] Because of their small size and high surface area-to-volume ratio, AuNPs exhibit special optical, electrical, and catalytic functions.[6] AuNPs/AuNCs are one of the most extensively studied nanomaterials in recent years due to their potential in a variety of applications. Consequently, there is an expanding amount of research on the synthesis, characteristics, and uses of AuNPs and AuNCs.

A number of investigations focused on the various aspects of the AuNP/AuNC interaction with biomolecular systems.[23−33] Kyriazi et al.[23] designed DNA-AuNP assemblies with multiple and synergistic functions, proposing the potential to advance sensing and drug delivery in cells. To understand the interactions of AuNPs with common blood proteins, an array of photophysical measurements were performed by Lacerda et

Received: September 3, 2023
Revised: December 20, 2023
Accepted: December 21, 2023
Published: January 8, 2024

al.[24] They reported that AuNPs strongly associate with essential blood proteins. Li et al.[25] in 2014 performed an antibacterial tactic for dealing with multidrug-resistant bacteria that uses self-therapeutic AuNPs. They reported that the correlation between the NP ligand structure and activity showed that surface chemistry had a significant impact on AuNP's antimicrobial capabilities, offering a design factor for forecasting and logically designing novel antibiotic NPs. The adsorption mechanism of oxygen on the isolated and nitrogen (N)-doped graphene monolayer supported by gold clusters was explored by density functional theory (DFT) calculations. The results showed that oxygen interacts with odd-numbered Au clusters stronger than even-numbered Au clusters.[26] An electrochemical sensor to expose tartrazine as a synthetic azo dye customarily found in commercial soft drinks was developed by Cardenas-Riojas et al. based on a carbon paste electrode with AuNPs anchored in carbon nanofibers.[27] Insights into the molecular interactions between small AuNCs with N = 6, 8, and 20 and 5-fluorouracil (5FU) anticancer drug were explored by means of DFT calculations by Ghazali et al.[28] Accordingly, the surface-enhanced Raman scattering (SERS) spectra of 5FU adsorbed on the Au surfaces show that the stretching vibrations of N−H and C=O bonds play a major role in the SERS phenomenon.[28] In another study, the potential of AuNCs for the delivery of the D-penicillamine anticancer drug was proposed by El-Mageed et al.[29] Moreover, the interactions of the Au_{13} NC and Au_{30} fullerene nanocage with nucleobases and amino acids were evaluated in detail by means of DFT calculations and MD simulations, respectively.[5,6] Nhat and co-workers carried out a theoretical investigation on pramipexole−Au cluster interactions for the applications of drug delivery and detection. Three AuNCs with sizes N = 6, 8, and 20 were used as reactant models to simulate the metallic nanostructured surfaces.[30] Shukla and co-workers[31] investigated the binding mechanism and molecular interactions of AuNCs with nucleic acid base guanine and the Watson−Crick guanine-cytosine base pair through DFT calculations. In their study, they considered AuNCs with sizes of 2, 4, 6, 8, 10, and 12 atoms. Sierpe et al. experimentally studied the interaction of the β-cyclodextrin phenylethylamine inclusion complex with AuNPs to understand photothermal drug release.[32] Recently, a theoretical study by Tandiana et al. reported the chemical interactions of aromatic compounds with AuNPs and predicted noncovalent interactions with dative, dispersive, and repulsive nature.[33]

The interactions of NPs with neurotransmitters, which are necessary for brain cell communication, are one of the attractive areas of research. The development of novel treatment strategies for neurological disorders can be improved by an understanding of how NPs interact with neurotransmitters. It has been found that the interaction of neurotransmitters with nanomaterials can change the neurotransmitters' functionality.[34−37] Epinephrine is an essential hormone, neurotransmitter, and medication. It is being produced by adrenal glands in the central nervous system.[38] Epinephrine plays crucial roles in fight to responses through increasing the level of pupil dilation and blood sugar.[39,40] This neurotransmitter is normally found in animals and some single-cell organisms.[41,42] It is worn in the treatment of anaphylaxis, superficial bleeding, and asthma.[43] Its abnormal use may lead to various side effects such as shakiness, anxiety, and sweating.[44,45] The involvement of nanotechnology in biology, nanomedicine, and scientific usefulness of epinephrine inspired us to perform a detailed in silico investigation on the interaction of the epinephrine neurotransmitter with AuNCs to explore deep insights into the molecular interactions involved between AuNCs and epinephrine and the potential application of AuNCs in the field of sensing and drug delivery applications for the diseases related to the epinephrine neurotransmitter.

2. COMPUTATIONAL DETAILS

Geometry optimization, vibrational frequency modes, and electronic structure calculations have been carried out using the DFT/B3LYP functional available in Gaussian09 suite without any symmetry restrictions.[46] The Lanl2DZ and 6-31++G(d,p) basis sets are applied for Au atoms and epinephrine molecules, respectively. The magnitude of adsorption energies for Au_nNC@epinephrine biomolecular conjugates has been computed using the following equation:

$$E_{ads} = E(\text{AuNC + epinephrine}) - E(\text{AuNC}) - E(\text{epinephrine}) + \text{BSSE} \quad (1)$$

where E (AuNC + epinephrine) represents the energy of AuNC@epinephrine. The E (AuNC)and E (epinephrine) terms represent the total energy of the isolated AuNC and epinephrine neurotransmitter, respectively. The counterpoise method is applied to correct the basis set superposition error (BSSE) for the adsorption energy. The energies of the individual components, namely, AuNCs and epinephrine, were individually optimized in their isolated forms. The negative adsorption energy implies a thermodynamically favorable complex. Furthermore, the Gibbs (free) energy[46] has been estimated from the following relation:

$$\Delta G^0(298) = \sum (\varepsilon_0 + G_{corr})_{Final} - \sum (\varepsilon_0 + G_{corr})_{Initial} \quad (2)$$

where $(\varepsilon_0 + G_{corr})$ is the addition of electronic and thermal free energies.

3. RESULTS AND DISCUSSION

Theoretical and experimental studies that provide insights into the molecular interactions of metal NPs or NCs with biomolecules are very crucial due to their involvement in various applications such as sensors, biomedical diagnostics, and many others.[47] The conformational and vibrational spectroscopic investigation of epinephrine was reported by us[45] already where we predicted possible low-lying energy conformers of epinephrine and its interaction with HCl to explore intermolecular hydrogen bonding. In addition, we also reported a natural bond orbital (NBO) analysis of both epinephrine and the epinephrine−HCl conjugate. Now, the interaction of epinephrine with even-numbered (n = 6, 8, and 10) Au clusters has been performed to explore the binding or adsorption mechanism of epinephrine with Au clusters, and the charge transfer is also being understood. The optimization of Au_nNC@epinephrine biomolecular conjugates by placing Au clusters at different possible interaction sites around epinephrine has been performed at the DFT/B3LYP/Lanl2DZ level/6-31++G(d,p) level. A wide range of positions and orientations of epinephrine relative to the clusters were applied. By systematically varying the initial positions and orientations of the epinephrine molecule, we aimed to cover the entire spatial region surrounding the clusters. Furthermore,

https://doi.org/10.1021/acsomega.3c06382
ACS Omega 2024, 9, 3373−3383

we performed multiple independent simulations with different starting configurations to enhance sampling of the conformational space. This approach allowed us to capture a diverse set of local minima and potentially identify the global minimum. Full geometry optimization ensued four possible configurations for each Au_nNC@epinephrine, i.e., a total of 12 possible configurations. These stable configurations have been considered for further investigation. Noticeably, all of the possible sites available in epinephrine while performing the interaction with all Au_n clusters were taken into account. The magnitude of adsorption energy is a crucial parameter for using an NC-based biomolecular complex in practical applications such as biosensing and life-saving medical treatments. Thus, the adsorption energy values for the considered configurations are computed and are listed in Table 1. The results infer the global minima for configurations of Au_6NC@epinephrine(a), Au_8NC@epinephrine(a), and Au_{10}NC@epinephrine(d) complexes. The optimized electronic structures of Au_6NC@epinephrine, Au_8NC@epinephrine, and Au_{10}NC@epinephrine biomolecular complexes with various prominent intermolecular contacts between Au_nNCs and the epinephrine neurotransmitter are shown in Figures 1, 2, and 3, respectively.

Table 1. Adsorption Energies for Various Configurations

configurations	E_{ads}(kcal/mol)
Au_6NC@epinephrine(a)	−17.45
Au_6NC@epinephrine(b)	−11.00
Au_6NC@epinephrine(c)	−7.53
Au_6NC@epinephrine(d)	−15.74
Au_8NC@epinephrine(a)	−17.86
Au_8NC@epinephrine(b)	−12.69
Au_8NC@epinephrine(c)	−9.31
Au_8NC@epinephrine(d)	−12.26
Au_{10}NC@epinephrine(a)	−14.75
Au_{10}NC@epinephrine(b)	−10.61
Au_{10}NC@epinephrine(c)	−7.23
Au_{10}NC@epinephrine(d)	−16.07

All the 12 possible configurations are simulated in the gas phase. Moreover, biomolecular complexes resulting from the interaction of Au_nNCs with epinephrine contain even-numbered electrons, so they offer a singlet multiplicity and neutral charge. The adsorption mechanism of AuNCs with biomolecules generally governs through the Au-X (X = N and O) anchoring bond and Au···H-X hydrogen bonding, which is conventional for Au complexes.[47] The Au-X (X = N and O) anchoring bond and Au···H-X hydrogen bonding play a significant role in the total adsorption energy because the Au interaction with X, i.e., N and O atoms, involves sharing of electrons, leading to the formation of a chemical bond, while Au···H-X hydrogen bonding can play a crucial role in the stabilization of the adsorbate on the metal surface. The Au_6 NC interacts with epinephrine via the Au−N anchoring bond, Au···H−C electrostatic bond, and Au···H−O hydrogen bonding with interaction distances of 2.29, 3.48, and 2.42 Å, respectively. For this configuration, the adsorption energies are computed to be −17.45 kcal/mol (without BSSE) and −13.83 kcal/mol including BSSE, which is higher than rest three configurations of Au_6NC@epinephrine biomolecular complexes. Configurations (b) and (d) involve a polar covalent Au_6−O bond and Au···H−C electrostatic bond, while configuration (c) stabilizes through Au···H−O hydrogen bonding and Au_6−O bond. These interactions play a crucial role in the stability of Au-based biomolecular complexes. In these configurations, the corresponding adsorption energies are −11.00, −7.53, and −15.74 kcal/mol. The adsorption energy calculations reveal that the Au_6 NC interacts more intensively

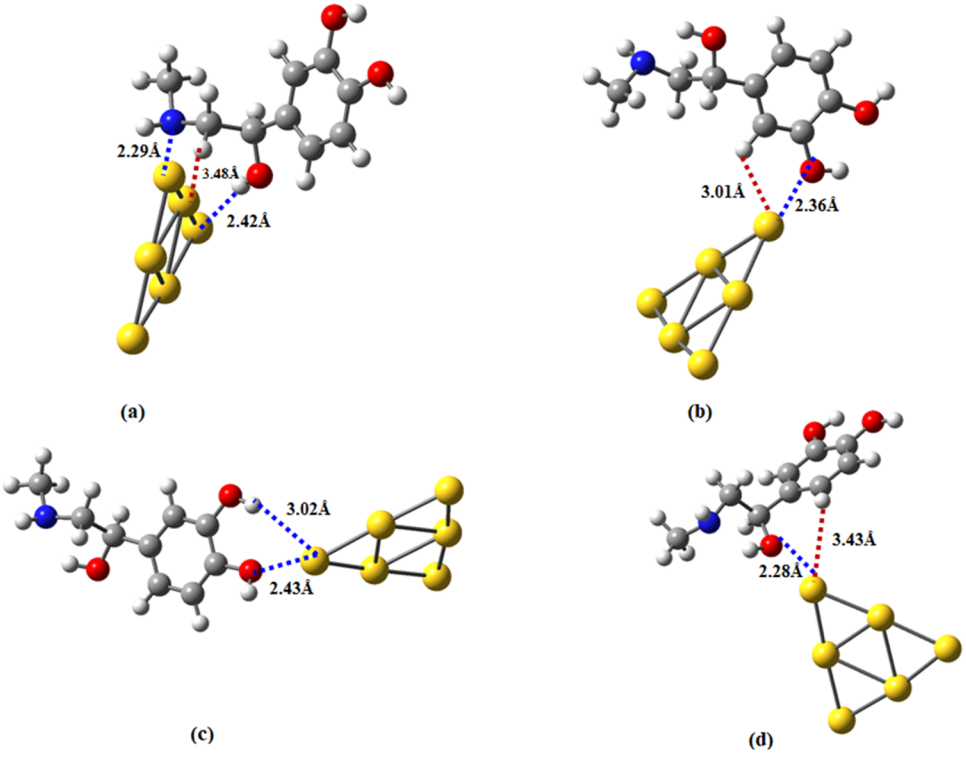

Figure 1. Optimized structures (a−d) of Au_6NC@epinephrine complexes for the various configurations.

https://doi.org/10.1021/acsomega.3c06382
ACS Omega 2024, 9, 3373−3383

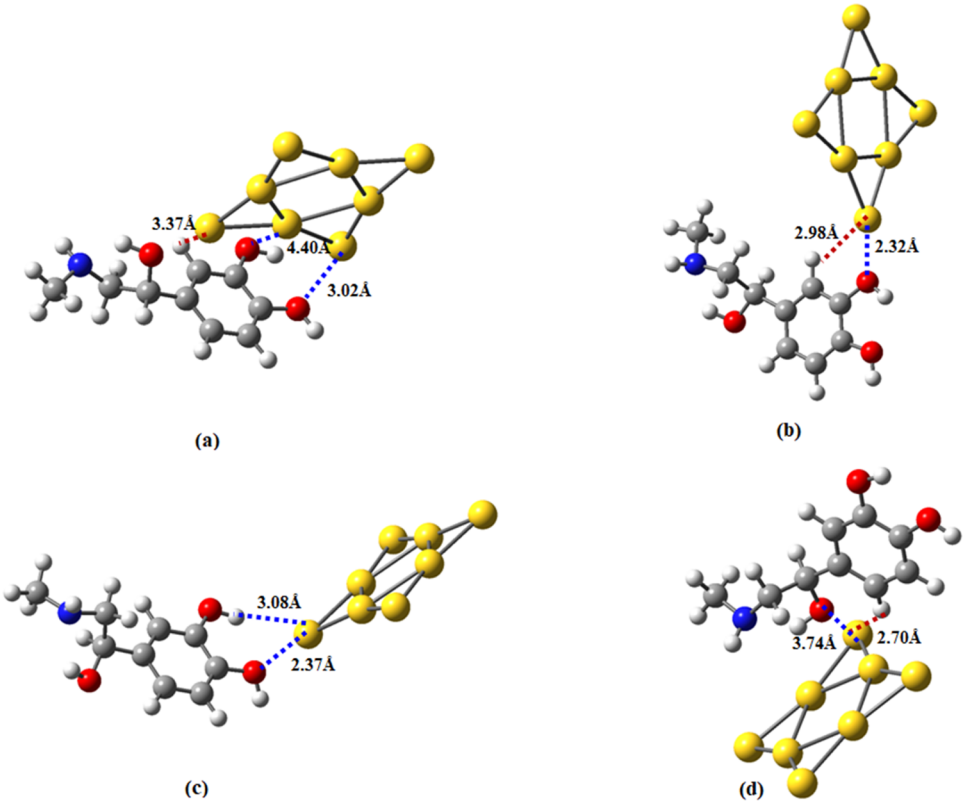

Figure 2. Optimized structures (a−d) of Au_8NC@epinephrine complexes for the various configurations.

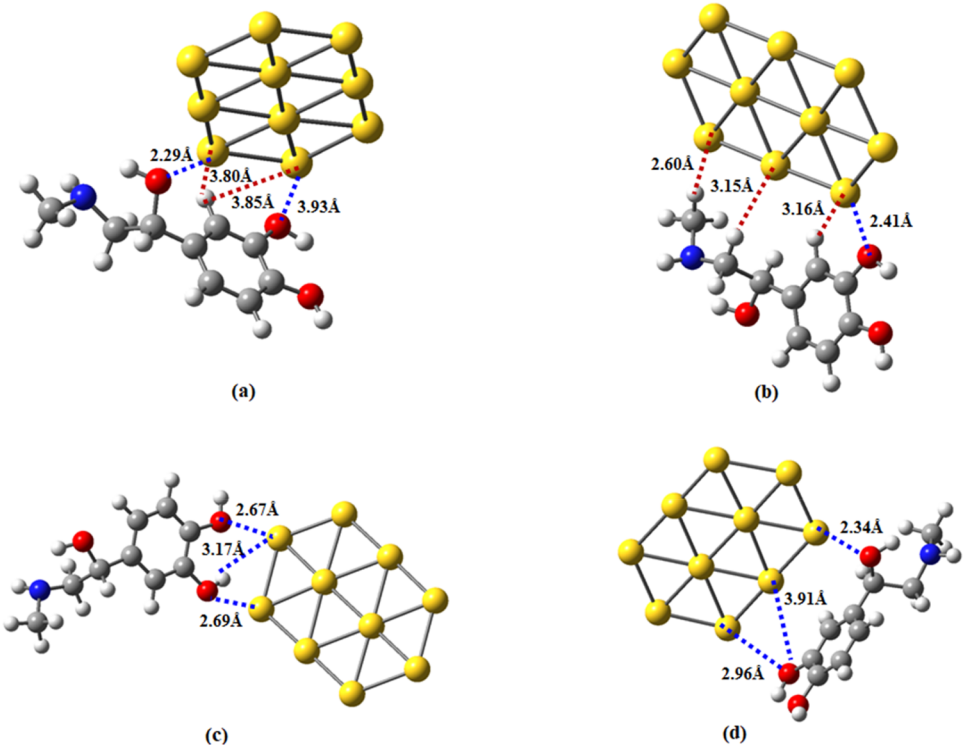

Figure 3. Optimized structures (a−d) of Au_{10}NC@epinephrine complexes for the various configurations.

with the side chain of epinephrine and prefers chemical adsorption. Moreover, the NBO analysis was performed through the NBO3.1 program of Gaussian09 to infer a charge transfer of 0.201e from epinephrine to the Au_6 cluster. Similar to the Au_6 NC, the interaction of Au_8 and Au_{10} clusters with epinephrine is stabilized via the Au−N anchoring bond, Au···H−C electrostatic bond, and Au···H−O hydrogen bonding. The magnitude of adsorption energy varies in the range of −9.31 to −17.86 kcal/mol for Au_8NC@epinephrine and −7.23 to −16.07 kcal/mol for the Au_{10}NC@epinephrine complex.

https://doi.org/10.1021/acsomega.3c06382
ACS Omega 2024, 9, 3373−3383

The remarkable adsorption energies of −17.86 and −16.07 kcal/mol without BSSE and −12.22 and −10.11 kcal/mol with BSSE for the most favorable adsorption configurations corresponding to the Au_8NC@epinephrine and Au_{10}NC@epinephrine biomolecular complexes further infer that the adsorption of AuNCs is chemical adsorption in nature. Furthermore, charge transfers of 0.404e and 0.173e take place from epinephrine to Au_8 and Au_{10} clusters, respectively. The adsorption energies of the most favorable configurations for the interaction of even-numbered gold clusters with epinephrine are in consistent with the earlier reported values for various nanomaterial-based biomolecular complexes,[48−50] which supports that the Au_nNC@epinephrine biomolecular complex can be utilized for different biological applications.

Some relevant electronic parameters, namely, highest occupied molecular orbital (HOMO) and lowest unoccupied molecular orbital (LUMO) energies, energy gap ($E_g = E_{LUMO} - E_{HOMO}$), and Fermi level ($E_F$) of Au_6, Au_8, Au_{10}, epinephrine, and all 12 possible Au_nNC@epinephrine complexes, are computed and summarized in Table 2. These

Table 2. Calculated HOMO Energy (E_H), LUMO Energy (E_L), HOMO−LUMO Energy Gap (E_g), Fermi Level Energy (E_F), and Work Function (ϕ)[a]

structure	E_H	E_L	E_g	E_F	Φ
epinephrine	−5.76	−0.14	5.62	−2.95	2.95
Au_6NC	−6.91	−3.43	3.48	−5.17	5.17
Au_8NC	−6.71	−3.94	2.77	−5.33	5.33
Au_{10}NC	−6.33	−4.06	2.27	−5.20	5.20
Au_6NC@epinephrine(a)	−6.06	−2.82	3.24	−4.44	4.44
Au_6NC@epinephrine(b)	−6.24	−2.87	3.37	−4.56	4.56
Au_6NC@epinephrine(c)	−6.28	−2.96	3.32	−4.62	4.62
Au_6NC@epinephrine(d)	−5.92	−2.65	3.27	−4.29	4.29
Au_8NC@epinephrine(a)	−5.84	−3.03	2.81	−4.44	4.44
Au_8NC@epinephrine(b)	−6.20	−3.34	2.86	−4.77	4.77
Au_8NC@epinephrine(c)	−6.29	−3.45	2.84	−4.87	4.87
Au_8NC@epinephrine(d)	−6.12	−3.41	2.71	−4.77	4.77
Au_{10}NC@epinephrine(a)	−5.46	−3.30	2.16	−4.38	4.38
Au_{10}NC@epinephrine(b)	−5.81	−3.62	2.19	−4.72	4.72
Au_{10}NC@epinephrine(c)	−5.69	−3.57	2.12	−4.63	4.63
Au_{10}NC@epinephrine(d)	−5.33	−3.11	2.22	−4.22	4.22

[a]All data are in eV.

are key parameters that can provide valuable information related to various properties including chemical reactivity and kinetic stability.[48] The schematic representation of isosurfaces corresponding to the HOMOs and LUMOs of the most favorable configurations of Au_6NC@epinephrine, Au_8NC@epinephrine, and Au_{10}NC@epinephrineare is depicted in Figure 4. This figure clearly shows that both the HOMOs and LUMOs in Au_6NC@epinephrine, Au_8NC@epinephrine, and Au_{10}NC@epinephrine are predominantly contributed by AuNCs. The magnitudes of energy of HOMOs and LUMOs in the most favorable configurations are computed to be −6.06 and −2.82 eV for Au_6NC@epinephrine, −5.84 and −3.03 eV for Au_8NC@epinephrine, and −5.33 and −3.11 eV for Au_{10}NC@epinephrine. Therefore, the corresponding energy gaps are 3.24, 2.81, and 2.22 eV. The energies of both HOMO and LUMO of the most favorable configurations become more unstable than isolated Au_6, Au_8, and Au_{10} AuNCs. As a result, the energy gaps significantly decrease in the case of Au_6NC@epinephrine and Au_{10}NC@epinephrine by 6.89 and 2.20% with respect to the isolated AuNCs. However, there is no significant change in energy gap upon the interaction of epinephrine with the Au_8NC. The decrement in energy gap in the case of Au_6NC@epinephrine and Au_{10}NC@epinephrine enhances the electrical conductivity (σ) in an exponential manner because the energy gap is directly proportional to the electrical conductivity accordingly:[51,52]

$$\sigma \propto \exp\left(\frac{-E_g}{2KT}\right) \tag{3}$$

where T and K stand for the absolute temperature and Boltzmann constant, respectively. Therefore, if the considered AuNCs are used as a portion of an electric circuit, it can produce an electrical signal, depending on the magnitude order of energy gap decrease after the epinephalue of Adsorption Energies for the M rine adsorption process. Therefore, the presence of epinephrine could be also determined based on its effect on the energy gap and thereby on the conductivity. Hence, epinephrine can be detected by converting the electrical conductivity into electrical signals.

The total densities of states (DOS) are utilized using GaussSum software[53] in evaluating the electronic structure of epinephrine adsorption on the surface of AuNCs. A basic representation of the properties of the molecular orbitals in a specific energy range is shown in Figure 5 along with a population analysis for each orbital. Based on the provided figure, a comparison of the DOS spectra between isolated gold clusters and AuNC@epinephrine complexes demonstrates that the presence of epinephrine leads to the destabilization and upward shift of both the HOMO and LUMO levels in the complexes relative to the isolated AuNCs. This adsorption-induced energy shift consequently alters the energy gap between the levels. Additionally, the DOS spectra reveal that epinephrine adsorption predominantly affects the occupied orbital energies, influencing both their occupation and energy, while having a lesser impact on the unoccupied orbitals.

It is critical to understand how AuNCs@epinephrine systems behave in aquatic environments in a number of disciplines, including biochemistry, nanotechnology, and materials science. We have adopted a polarizable continuum model[54] to evaluate the effect of the aqueous medium on the interaction of Au_nNCs with the epinephrine molecule. The adsorption energies (Table 3) in the water phase for the most favorable configurations of Au_6NC@epinephrine, Au_8NC@epinephrine, and Au_{10}NC@epinephrine have been computed to be −16.73, −15.39, and −13.14 kcal/mol, respectively, indicating a decrement in the adsorption energies in the water phase. Moreover, the negative sign reveals that the adsorption process of epinephrine over the AuNCs surface is of a spontaneous nature. The HOMO−LUMO energies, energy gap, and Fermi energy values in the aqueous phase are listed in Table 4. This table infers that the energy gaps increase by a little amount for all three most favorable configurations of Au_6NC@epinephrine, Au_8NC@epinephrine, and Au_{10}NC@epinephrine by 0.06, 0.19, and 0.08 eV, respectively. However, this change is more significant for Au_8NC@epinephrine in comparison to Au_6NC@epinephrine and Au_{10}NC@epinephrine. The increment in the energy gap of Au_8NC@epinephrine by 0.19 eV is noteworthy, and it infers a slight decrement in reactivity in the aqueous phase compared to the gas phase. In addition, the dipole moments are computed to be 7.78, 11.60, and 13.62 D in the gas phase for the most favorable

https://doi.org/10.1021/acsomega.3c06382
ACS Omega 2024, 9, 3373−3383

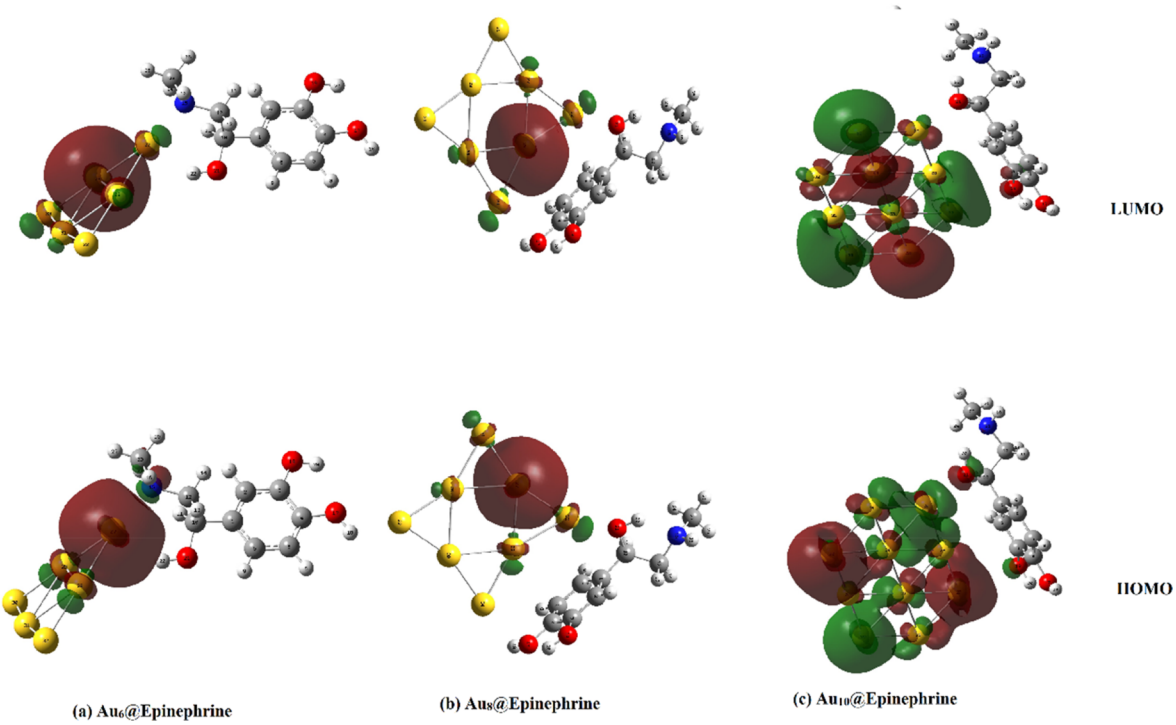

Figure 4. (a–c) HOMO and LUMO isosurfaces of Au_6NC@epinephrine, Au_8NC@epinephrine, and Au_{10}NC@epinephrine in the most stable configurations.

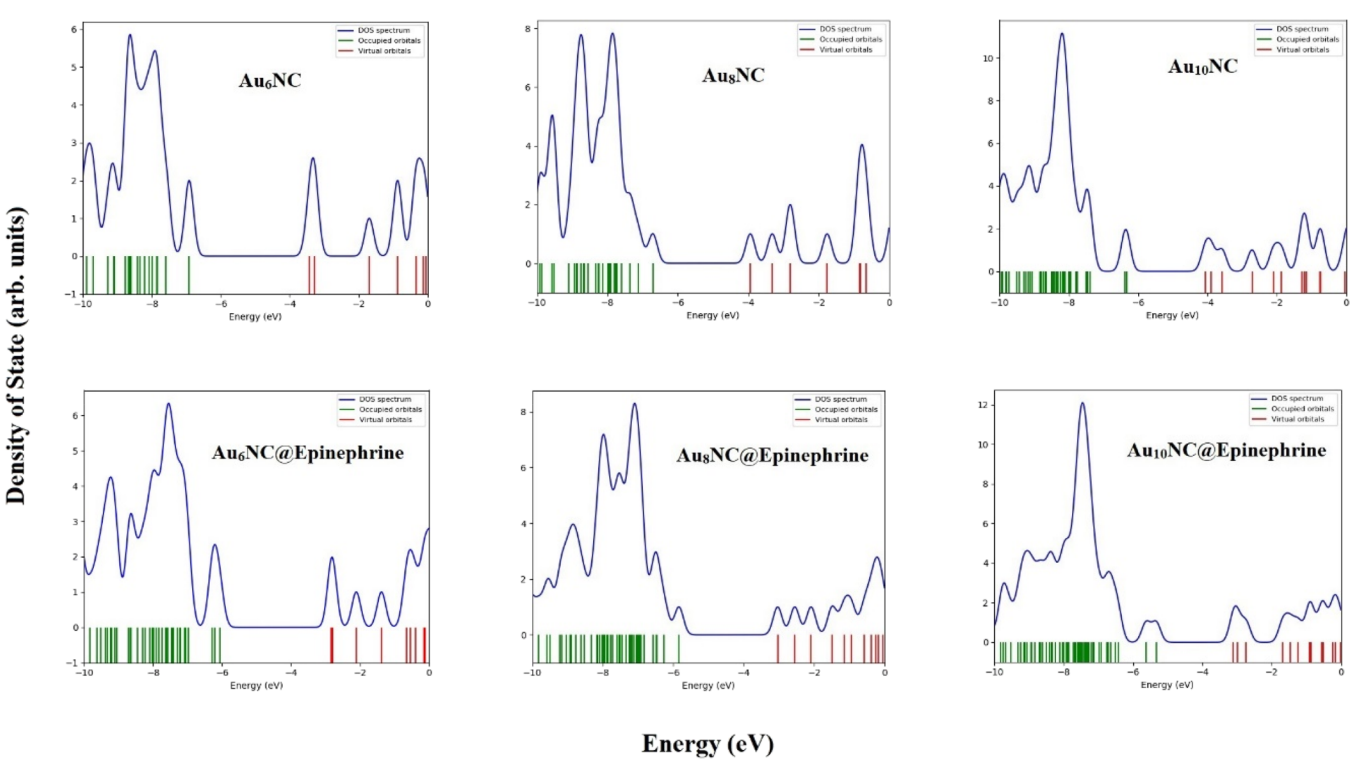

Figure 5. DOS for Au_6NC, Au_8NC, Au_{10}NC, Au_6NC@epinephrine, Au_8NC@epinephrine, and Au_{10}NC@epinephrine complexes.

configurations of Au_6NC@epinephrine, Au_8NC@epinephrine, and Au_{10}NC@epinephrine, respectively. However, these increase by 2.83, 2.32, and 4.75 D in the aqueous phase, respectively. Thus, the symmetry arrangements of configurations are also influenced by the impact of the aqueous medium. Also, the increment of dipole moment infers an improved solubility of the above-cited configurations. Furthermore, the Gibbs (free) energy has been calculated for all the three most favorable configurations in gas and aqueous phases as well. The values of Gibbs (free) energy are −6.23, −4.29, and −2.48 kcal/mol in the gas phase while −3.85, 0.46, and −2.47 kcal/mol in the aqueous phase for the most favorable configurations. The negative sign infers an exergonic interaction of epinephrine with AuNCs.

https://doi.org/10.1021/acsomega.3c06382
ACS Omega 2024, 9, 3373−3383

Table 3. Value of Adsorption Energies for the Most Favorable Configurations in the Aqueous Phase

configurations	E_{ads}(kcal/mol)
Au_6NC@epinephrine(a)	−16.73
Au_8NC@epinephrine(a)	−15.39
Au_{10}NC@epinephrine(d)	−13.14

Table 4. Calculated HOMO Energy (E_H), LUMO Energy (E_L), HOMO−LUMO Energy Gap (E_g), Fermi Level Energy (E_F), and Work Function (ϕ) in the Aqueous Phase[a]

structure	E_H	E_L	E_g	E_F	Φ
epinephrine	−6.02	−0.38	5.64	−3.20	3.20
Au_6NC	−6.26	−2.59	3.67	−4.43	4.43
Au_8NC	−6.11	−3.14	2.97	−4.63	4.63
Au_{10}NC	−5.61	−3.27	2.34	−4.44	4.44
Au_6NC@epinephrine(a)	5.85	−2.55	3.30	−4.20	4.20
Au_8NC@epinephrine(a)	−5.87	−2.87	3.00	−4.37	4.37
Au_{10}NC@epinephrine(d)	−5.27	−2.97	2.30	−4.12	4.12

[a]All data are in eV.

The electron localization function (ELF) is a crucial computational chemistry tool utilized for both quantitative and visual analyses of electron distribution within molecules. It offers a precise quantitative evaluation of electron localization or delocalization, achieved through mathematical analysis of electron density.[55,56] In this study, we generated ELF maps using Multiwfn software[57] from the optimized structure of the Au_6NC@epinephrine, Au_8NC@epinephrine, and Au_{10}NC@epinephrine. This method reveals areas with varying electron concentrations, effectively characterizing the nature of the chemical bonds. ELF, by delineating electron sharing or localization, provides invaluable insights into the electronic structure, thereby enhancing comprehension of molecular behavior, reactivity, and bonding patterns. Its particular strength lies in elucidating intricate systems, rendering ELF an indispensable asset for researchers in the fields of quantum chemistry and materials science. The ELF maps of Au_6NC@epinephrine, Au_8NC@epinephrine, and Au_{10}NC@epinephrine are depicted in Figure 6. In these ELF maps, the red hues denoted the areas of a higher electron density, highlighting pronounced electron localization in specific molecular regions. Notably, these red regions were predominantly concentrated around hydrogen atoms, suggesting a significant accumulation of localized electrons in their vicinity. This finding offers valuable insights into the electron-rich nature of chemical bonds involving hydrogen. In contrast, the blue areas on the ELF maps indicated the regions with a lower electron density, signifying a higher degree of electron delocalization. The electron cloud delocalized around some carbon and Au atoms (C2 and C10) and (C10, C23, and all Au atoms) is represented by the blue regions in Au_6NC@epinephrine and Au_8NC@epinephrine. However, in the case of Au_{10}NC@epinephrine, the delocalization of the electron cloud is at (C6, C2, Au28, Au29, Au30, Au31, Au32, Au33, Au34, and Au35). The sites at (H7, H11, H24, and H26) and (H8, H11, H14, H18, H22, H25, and H26) show a strong electronic localization for Au_6NC@epinephrine and Au_8NC@epinephrine. However, in the case of Au_{10}NC@epinephrine, the location of the electron cloud is at (H13, H14, and H26) sites.

The total and vibrational contributions of some standard thermodynamical parameters such as thermal energy, entropy, and specific heat have been computed as these help in estimating the direction of chemical reactions and per the second law of thermodynamics.[58] The magnitudes of the corresponding parameters are listed in Table 5. A perusal of this table infers that thermal energies and specific heats in the case of the most favorable configurations of Au_6NC@epinephrine, Au_8NC@epinephrine, and Au_8NC@epinephrine are predominately contributed due to the vibrational motion in both gas and aqueous phases. However, in the case of the entropy of these systems, the electronic and rotational motion is equally involved in addition with vibrational motion. Moreover, the zero point vibrational energies (ZPVE) are computed to be 137.698, 138.163, and 138.738 kcal/mol, respectively, in the gas phase, and there are no significant changes on ZPVE seen in the aqueous phase.

The thermal stability of the most stable complexes is studied in a box of 25 × 25 × 25 Å with an NVT ensemble at 300 K with a time step of 1 fs in 3000 steps with a massive generalized Gaussian moment thermostat utilizing the molecular dynamics (MD) simulations actualized in the DMol^3 module. In the NVT ensemble, N, V, and T are a steady number of atoms, volume, and temperature, respectively. The obtained results presented in Figure 7 approved the thermal stability of the Au_n@epinephrine complexes. Fluctuation of the total energy that is a criterion for the thermal stability of the studied systems is less than 0.002 Ha for the considered Au_n@epinephrine complexes. Thus, the structure is structurally and dynamically stable under the studied conditions. In other words, the desired structure has no structural and dynamic changes after this time in the imposed

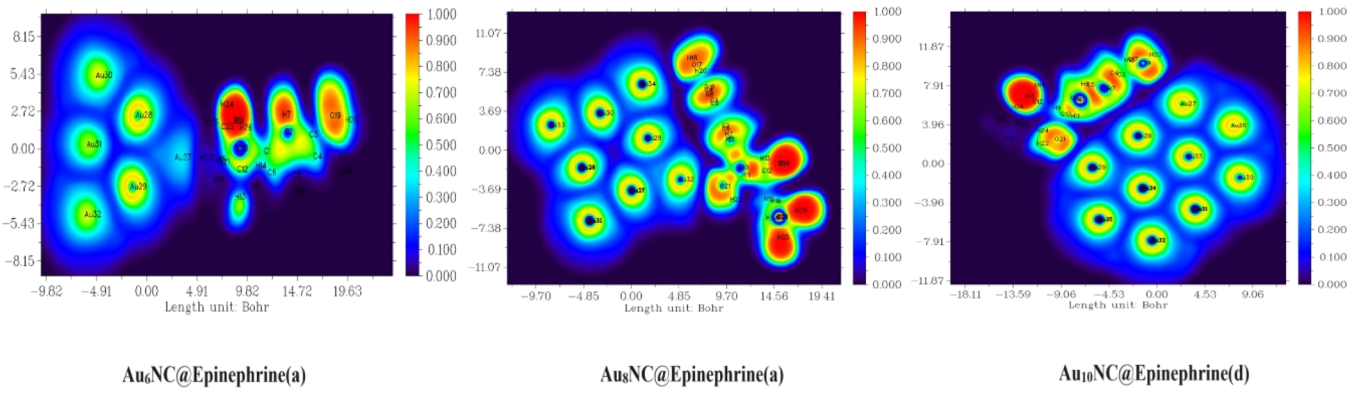

Figure 6. ELF plots of the Au_6NC@epinephrine, Au_8NC@epinephrine, and Au_{10}NC@epinephrine complexes.

https://doi.org/10.1021/acsomega.3c06382
ACS Omega 2024, 9, 3373−3383

Table 5. Some Standard Thermodynamical Parameters of Au_6NC@Epinephrine(a), Au_8NC@Epinephrine(a), and Au_{10}NC@Epinephrine(d)

	Au_6NC@epinephrine(a)		Au_8NC@epinephrine(a)		Au_{10}NC@epinephrine(d)	
parameters	gas phase	aqueous phase	gas phase	aqueous phase	gas phase	aqueous phase
thermal energy (kcal/mol)	154.717 (152.939)	154.705 (152.927)	158.226 (156.449)	157.916 (156.138)	161.824 (160.046)	161.484 (159.707)
specific heat (CV) (cal/(mol K))	84.761 (78.800)	84.819 (78.857)	96.083 (90.121)	95.576 (89.615)	107.857 (101.895)	107.556 (101.595)
entropy (S) (cal/(mol K))	214.924 (128.085)	210.061 (123.249)	242.151 (153.911)	235.666 (147.452)	269.219 (179.537)	265.885 (176.196)
ZPVE (kcal/mol)	137.698	137.713	138.163	138.073	138.738	138.527

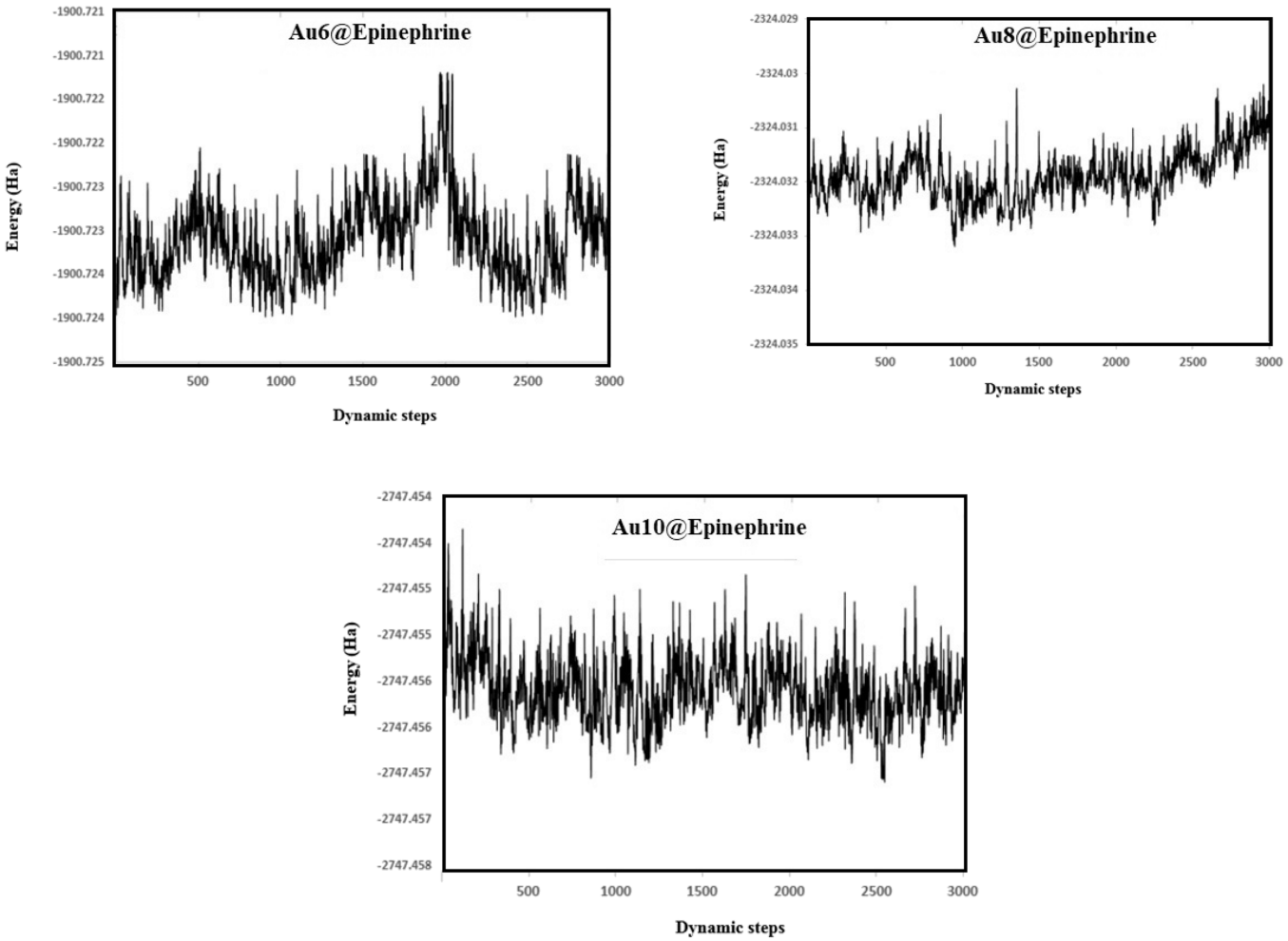

Figure 7. Alterations of the total energy (NVT) vs dynamic steps in the MD simulation at 300 K for the Au_nNC@epinephrine complexes.

conditions and has thermal stability. So, the thermal stability of these systems is confirmed at 300 K.

This study also explores NBO calculations for the interaction of epinephrine with Au_6, Au_8, and Au_{10} NCs. The second-order Fock matrix was employed to determine the donor−acceptor interactions in the NBO. The formula of the second-order perturbation approach was used to deduce the hyperconjugative energy ($E^{(2)}$).[59−62] Relevant transitions and corresponding interaction energies of core and lone pair orbitals to antibonding orbitals are considered and collected in Table S1, respectively. NBO analysis is a powerful technique for investigating intra- and intermolecular bonding interactions. It is also an important framework for studying charge transfer or conjugative interactions in molecular systems. Intramolecular interactions are formed through the overlap of bonding and antibonding orbitals, resulting in intramolecular charge transfer and system stabilization.[63] The energy required for the stabilization of the various allowed transitions within bonding and antibonding levels is referred to as hyperconjugative energy. The transitions with the highest magnitude of hyperconjugative energy ($E^{(2)}$) are considered to be the most probable compared to other transitions.

In Au_6NC@epinephrine, the following transitions exhibit interaction energies: LP2(O19) → π^*(C2−C3) (25.70 kcal/mol), LP2(O17) → π^*(C4−H5) (21.81 kcal/mol), LP2(O21) → σ^*(C10−C12) (7.69 kcal/mol), LP1(O19) → σ^*(C3−C4) (6.92 kcal/mol), LP1(O17) → σ^*(C4−C5) (6.50 kcal/mol), and LP1(N15) → σ^*(C23−H26) (4.23 kcal/mol). These

https://doi.org/10.1021/acsomega.3c06382
ACS Omega 2024, 9, 3373−3383

findings indicate that the LP2(O19) → π*(C2−C3) transition is particularly strong, resulting in a significant charge transfer between them. In Au_8NC@epinephrine, the most probable transitions are LP2(O19) → π*(C2−C3) (26.11 kcal/mol), LP2(O17) → π*(C4−H5) (21.07 kcal/mol), LP1(O19) → σ*(C3−C4) (7.21 kcal/mol), LP1(N15) → σ*(C23−H26) (6.63 kcal/mol), LP1(O17) → σ*(C4−C5) (6.20 kcal/mol), LP1(O21) → σ*(C10−H11) (6.12 kcal/mol), and LP1(N15) → σ*(C12−H14) (5.70 kcal/mol). These transitions have hyperconjugative energy ($E^{(2)}$) values associated with them. Moreover, in Au_{10}NC@epinephrine, the intensive transitions are LP2(O19) → π*(C3−C4) (24.62 kcal/mol), LP2(O17) → π*(C3−C4) (20.29 kcal/mol), LP1(N15) → σ*(O21−H22) (15.21 kcal/mol), LP1(N15) → σ*(C23−H26) (6.70 kcal/mol), LP1(O19) → σ*(C3−C4) (6.69 kcal/mol), LP1(O17) → σ*(C4−C5) (6.67 kcal/mol), and LP1(N15) → σ*(C12−H14) (5.87 kcal/mol).

Table S1 provides the $E^{(2)}$ energy values for the interactions between epinephrine and Au atoms. In Au_6NC@epinephrine, there are intense transitions such as LP1(N15) → LP6(Au27) (44.66 kcal/mol) and LP1(N15) → LP*7(Au27) (10.35 kcal/mol). Similarly, in Au_8NC@epinephrine, notable transitions include LP3(O19) → LP*1(H20) (474.95 kcal/mol), LP3(O17) → LP*1(H18) (473.08 kcal/mol), LP3(O21) → LP*1(H22) (391.85 kcal/mol), LP2(O21) → LP*6(Au32) (23.88 kcal/mol), and LP2(O21) → LP*6(Au32) (5.51 kcal/mol). Finally, in Au_{10}NC@epinephrine, the highly intense transitions are LP2(O21) → LP*6(Au29) (21.20 kcal/mol), LP2(O19) → LP6(Au27) (3.34 kcal/mol), and π(C1−C2) → LP*6(Au28) (7.08 kcal/mol). Moreover, the adsorption energies for the most stable configurations in the gas phase are computed using the Lanl2DZ and 6-311++G(d,p) basis sets, and the results are given in the Supporting Information.

4. CONCLUSIONS

In conclusion, this study focused on optimizing the Au_nNC@epinephrine biomolecular conjugates by exploring various configurations through DFT simulations. By systematically varying the positions and orientations of epinephrine relative to the gold clusters, multiple stable configurations were identified, and their adsorption energies were computed. The results revealed that the most favorable configurations were Au_6NC@epinephrine(a), Au_8NC@epinephrine(a), and Au_{10}NC@epinephrine(d), indicating the presence of strong chemical adsorption between the clusters and epinephrine. The computed adsorption energies and charge transfer values support the potential use of these biomolecular complexes in various biological applications. This study investigated the electronic parameters and electronic structures of AuNC@epinephrine complexes. The computed values for HOMO, LUMO, and the energy gap showed that the presence of epinephrine significantly influenced the electronic properties of the complexes. Specifically, the energy gap decreased, leading to an increased electrical conductivity. These findings suggest that these complexes can be used for the detection of epinephrine based on changes in electrical conductivity. The analysis of the total DOS further supported these observations. AuNCs@epinephrine systems were studied in aquatic environments by using computational methods. The adsorption energies of Au_6NC@epinephrine, Au_8NC@epinephrine, and Au_{10}NC@epinephrine in water were found to be −16.73, −15.39, and −13.14 kcal/mol, respectively. The adsorption process was spontaneous. Energy gaps increased slightly in the aqueous phase, indicating a decreased reactivity. Dipole moments and solubility also increased. Gibbs (free) energy values confirmed the exergonic interaction. MD simulations showed a good thermal stability of these at 300 K. Overall, this study provides insights for the development of sensing technologies for epinephrine detection.

■ ASSOCIATED CONTENT

Supporting Information

The Supporting Information is available free of charge at https://pubs.acs.org/doi/10.1021/acsomega.3c06382.

(Tables S1 and S2) Second-order perturbation theory analysis and adsorption energies for the most stable configurations using the B3LYP/6-311++(d,p) level of theory (PDF)

■ AUTHOR INFORMATION

Corresponding Authors

Nagendra Prasad Yadav − *School of Electrical and Electronics Information Engineering, Hubei Polytechnic University, Huangshi, Hubei 435003, China*; orcid.org/0000-0001-8932-4607; Email: npycn@hbpu.edu.cn

Subhendu Chakroborty − *Department of Basic Sciences, IITM, IES University, Bhopal, MP 462044, India*; Email: subhendu.cy@gmail.com

Anil Kumar Vishwkarma − *Department of Physics, Institute of Science, Banaras Hindu University, Varanasi 221005, India*; Email: akv1993.au@gmail.com

Authors

Tarun Yadav − *Department of Basic Sciences, IITM, IES University, Bhopal, MP 462044, India*

Sangram Pattanaik − *Sri Satya Sai University of Technology & Medical Sciences, Sehore, MP 466002, India*

Ehsan Shakerzadeh − *Chemistry Department, Faculty of Science, Shahid Chamran University of Ahvaz, Ahwaz 6135783151, Iran*

Cai Xiaofeng − *School of Electrical and Electronics Information Engineering, Hubei Polytechnic University, Huangshi, Hubei 435003, China*

Amit Pathak − *Department of Physics, Institute of Science, Banaras Hindu University, Varanasi 221005, India*

Jitendra Malviya − *Department of Life Sciences and Biological Sciences, IES University, Bhopal, MP 462044, India*

Fanindra Pati Pandey − *Scitechesy Research and Technology Private Limited, Central Discovery Center, Banaras Hindu University, Varanasi 221005, India*

Complete contact information is available at: https://pubs.acs.org/10.1021/acsomega.3c06382

Notes

The authors declare no competing financial interest.

■ ACKNOWLEDGMENTS

Nagendra Prasad Yadav is grateful for support through project no. 501-120221062060 Hubei Polytechnic University Laboratory Funds and Natural Science Foundation of Hubei Province (2023AFD008) and Science and Technology Talents Service Enterprise Project (KJRQ2023000110). Fanindra Pati Pandey acknowledges the financial support from BIRAC−DBT in the form of project (BIRAC/CCAMP01879/BIG-21/22). Anil Kumar Vishwkarma is grateful to UGC India for financial

support in form of UGC-JRF/SRF (Award Number: 1499/(CSIR-UGC NET DEC. 2018)). Amit Pathak also acknowledges support from Core Rsearch Grant of SERB, New Delhi (CRG/2021/000907).

REFERENCES

(1) Gawande, M. B.; Goswami, A.; Felpin, F. X.; Asefa, T.; Huang, X.; Silva, R.; Zou, X.; Zboril, R.; Varma, R. S. Cu and Cu-Based Nanoparticles: Synthesis and Applications in Catalysis. *Chem. Rev.* **2016**, *116*, 3722−3811.

(2) Morita, M.; Tachikawa, T.; Seino, S.; Tanaka, K.; Majima, T. Controlled Synthesis of Gold Nanoparticles on Fluorescent Nanodiamond via Electron-Beam-Induced Reduction Method for Dual-Modal Optical and Electron Bioimaging. *ACS Appl. Nano Mater.* **2018**, *1*, 355−363.

(3) Sagle, L. B.; Ruvuna, L. K.; Bingham, J. M.; Liu, C.; Cremer, P. S.; Van Duyne, R. P. Single Plasmonic Nanoparticle Tracking Studies of Solid Supported Bilayers with Ganglioside Lipids. *J. Am. Chem. Soc.* **2012**, *134* (38), 15832−15839.

(4) Banjare, M. K.; Behera, K.; Banjare, R. K.; Sahu, R.; Sharma, S.; Pandey, S.; Satnami, M. L.; Ghosh, K. K. Interaction of ionic liquid with silver nanoparticles: potential application in induced structural changes of globular proteins. *ACS Sustain. Chem. & Engin.* **2019**, *7* (13), 11088−11100.

(5) Darvish Ganji, M.; Tavassoli Larijani, H.; Alamol-hoda, R.; Mehdizadeh, M. First-principles and Molecular Dynamics simulation studies of functionalization of Au32 golden fullerene with amino acids. *Sci. Rep.* **2018**, *8*, 11400.

(6) Hashemkhani Shahnazari, G.; Darvish Ganji, M. Understanding structural and molecular properties of complexes of nucleobases and Au13 golden nanocluster by DFT calculations and DFT-MD simulation. *Sci. Rep.* **2021**, *11*, 435.

(7) Dauthal, P.; Mukhopadhyay, M. Noble Metal Nanoparticles: Plant-Mediated Synthesis, Mechanistic Aspects of Synthesis, and Applications. *Ind. Eng. Chem. Res.* **2016**, *55*, 9557−9577.

(8) Gholami, A.; Shakerzadeh, E.; Chigo Anota, E. Exploring the potential use of pristine and metal-encapsulated B36N36 fullerenes in delivery of β-lapachone anticancer drug: DFT approach. *Polyhedron* **2023**, *232*, No. 116295.

(9) Ando, J.; Nakamura, A.; Yamamoto, M.; Song, C.; Murata, K.; Iino, R. Multicolor High-Speed Tracking of Single Biomolecules with Silver, Gold, and Silver−Gold Alloy Nanoparticles. *ACS Photonics* **2019**, *6*, 2870−2883.

(10) Gallegos, F. E.; Meneses, L. M.; Cuesta, S. A.; Santos, J. C.; Arias, J.; Carrillo, P.; Pilaquinga, F. Computational Modeling of the Interaction of Silver Clusters with Carbohydrates. *ACS Omega* **2022**, *7*, 4750−4756.

(11) Barbir, R.; Jiménez, R. R.; Martín-Rapún, R.; Strasser, V.; Domazet Jurašin, D.; Dabelič, S.; de la Fuente, J. M.; Vinkovič Vrcček, I. Interaction of Differently Sized, Shaped, and Functionalized Silver and Gold Nanoparticles with Glycosylated versus Nonglycosylated Transferrin. *ACS Appl. Mater. Interfaces* **2021**, *13*, 27533−27547.

(12) Yeh, C. H.; Hsiao, Y. J.; Jiang, J. C. Dopamine sensing by boron and nitrogen co-doped single-walled carbon nanotubes: A first-principles study. *Appl. Surf. Sci.* **2019**, *473*, 59−64.

(13) Urdaneta, I.; Keller, A.; Atabek, O.; Palma, J. L.; Finkelstein-Shapiro, D.; Tarakeshwar, P.; Mujica, V.; Calatayud, M. Dopamine Adsorption on TiO2 Anatase Surfaces. *J. Phys. Chem. C* **2014**, *118*, 20688−20693.

(14) Barbir, R.; Jiménez, R. R.; Martín-Rapún, R.; Strasser, V.; Domazet Jurašin, D.; Dabelič, S.; de la Fuente, J. M.; Vinkovič Vrček, I. Interaction of Differently Sized, Shaped, and Functionalized Silver and Gold Nanoparticles with Glycosylated versus Nonglycosylated Transferrin. *ACS Appl. Mater. Interfaces* **2021**, *13*, 27533−27547.

(15) Fahy, K. M.; Eiken, M. K.; Baumgartner, K. V.; Leung, K. Q.; Anderson, S. E.; Berggren, E.; Bouzos, E.; Schmitt, L. R.; Asuri, P.; Wheeler, K. E. Silver Nanoparticle Surface Chemistry Determines Interactions with Human Serum Albumin and Cytotoxic Responses in Human Liver Cells. *ACS Omega* **2023**, *8*, 3310−3318.

(16) Venkatesh, G.; Sixto-López, Y.; Vennila, P.; Mary, Y. S.; Correa-Basurto, J.; Mary, Y. S.; Manikandan, A. An investigation on the molecular structure, interaction with metal clusters, anti-Covid-19 ability of 2-deoxy-D-glucose: DFT calculations, MD and docking simulations. *J. Mol. Struct.* **2022**, *1258*, No. 132678.

(17) Li, Y.; Hodak, M.; Lu, W.; Bernholc, J. Selective sensing of ethylene and glucose using carbon-nanotube-based sensors: an ab initio investigation. *Nanoscale* **2017**, *9*, 1687−1698.

(18) Khlebtsov, N.; Bogatyrev, V.; Dykman, L.; Khlebtsov, B.; Staroverov, S.; Shirokov, A.; Matora, L.; Khanadeev, V.; Pylaev, T.; Tsyganova, N.; Terentyuk, G. Analytical and Theranostic Applications of Gold Nanoparticles and Multifunctional Nanocomposites. *Teranostics* **2013**, *3*, 167−180.

(19) Paciotti, G. F.; Myer, L.; Weinreich, D.; Goia, D.; Pavel, N.; McLaughlin, R. E.; Tamarkin, L. Colloidal Gold: A Novel Nanoparticle Vector for Tumor Directed Drug Delivery. *Drug Delivery* **2004**, *11*, 169−183.

(20) Connor, E. E.; Mwamuka, J.; Gole, A.; Murphy, C. J.; Wyatt, M. D. Gold Nanoparticles Are Taken Up by Human Cells but Do Not Cause Acute Cytotoxicity. *Nano. Mic. Small* **2005**, *1*, 325−327.

(21) Giljohann, D. A.; Seferos, D. S.; Daniel, W. L.; Massich, M. D.; Patel, P. C.; Mirkin, C. A. Gold Nanoparticles for Biology and Medicine. *Angew. Chem., Int. Ed.* **2010**, *49*, 3280−3294.

(22) Zhang, X. D.; Luo, Z.; Chen, J.; Wang, H.; Song, S. S.; Shen, X.; Long, W.; Sun, Y. M.; Fan, S.; Zheng, K.; Leong, D. T.; Xie, J. Storage of Gold Nanoclusters in Muscle Leads to their Biphasic in Vivo Clearance. *Nano. Mic. Small* **2015**, *11*, 1683−1690.

(23) Kyriazi, M. E.; Giust, D.; El-Sagheer, A. H.; Lackie, P. M.; Muskens, O. L.; Brown, T.; Kanaras, A. G. Multiplexed mRNA Sensing and Combinatorial-Targeted Drug Delivery Using DNA-Gold Nanoparticle Dimers. *ACS Nano* **2018**, *12*, 3333−3340.

(24) Lacerda, S. H. De P.; Park, J. J.; Meuse, C.; Pristinski, D.; Becker, M. L.; Karim, A.; Douglas, J. F. Interaction of Gold Nanoparticles with Common Human Blood Proteins. *ACS Nano* **2010**, *4*, 365−379.

(25) Li, X.; Robinson, S. M.; Gupta, A.; Saha, K.; Jiang, Z.; Moyano, D. F.; Sahar, A.; Riley, M. A.; Rotello, V. M. Functional Gold Nanoparticles as Potent Antimicrobial Agents against Multi-Drug-Resistant Bacteria. *ACS Nano* **2014**, *8*, 10682−10686.

(26) Chen, X.; Sun, S.; Li, F.; Wang, X.; Xia, D. The Interactions of Oxygen with Small Gold Clusters on Nitrogen-Doped Graphene. *Molecules* **2013**, *18*, 3279−3291.

(27) Cardenas-Riojas, A. A.; Calderon-Zavaleta, S. L.; Quiroz-Aguinaga, U.; López, E. O.; Ponce-Vargas, M.; Baena-Moncada, A. M. Evaluation of an electrochemical sensor based on gold nanoparticles supported on carbon nanofibers for detection of tartrazine dye. *J. Sol. Sta. Electchem.* **2023**, *27*, 1969−1982.

(28) Ghazali, F.; Hosseini, S.; Ketabi, S. DFT and Molecular Simulation Study of Gold Clusters as Effective Drug Delivery Systems for 5-Fluorouracil Anticancer Drug. *J. Clust. Sci.* **2023**, *34*, 1499−1509.

(29) El-Mageed, H. R. A.; Mustafa, F. M.; Abdel-Latif, M. K. The ability of gold nanoclusters as a new nanocarrier for D-penicillamine anticancer drug: a computational chemistry study. *Struct. Chem.* **2020**, *31*, 781−793.

(30) Si, N. T.; Nhung, N. T. A.; Bui, T. Q.; Nguyen, M. T.; Nhat, P. V. Gold nanoclusters as prospective carriers and detectors of pramipexole. *RSC Adv.* **2021**, *11*, 16619−16632.

(31) Shukla, M. K.; Dubey, M.; Zakar, E.; Leszczynski, J. DFT Investigation of the Interaction of Gold Nanoclusters with Nucleic Acid Base Guanine and the Watson−Crick Guanine-Cytosine Base Pair. *J. Phys. Chem. C* **2009**, *113*, 3960−3966.

(32) Sierpe, R.; Lang, E.; Jara, P.; Guerrero, A. R.; Chornik, B.; Kogan, M. J.; Yutronic, N. Gold Nanoparticles Interacting with β-Cyclodextrin−Phenylethylamine Inclusion Complex: A Ternary System for Photothermal Drug Release. *ACS Appl. Mater. Interfaces* **2015**, *7*, 15177−15188.

https://doi.org/10.1021/acsomega.3c06382
ACS Omega 2024, 9, 3373−3383

(33) Tandiana, R.; Sicard-Roselli, C.; Van-Oanh, N. T.; Steinmann, S.; Clavaguéra, C. In-depth theoretical understanding of the chemical interaction of aromatic compounds with a gold nanoparticle. *Phys. Chem. Chem. Phys.* **2022**, *24*, 25327.
(34) Zestos, A. G. Zestos, Carbon Nanoelectrodes for the Electrochemical Detection of Neurotransmitters. *Int. J. Electrochem.* **2018**, *2018*, 3679627.
(35) Fuentes, V. M.; Mayer, A. B.; Lima, M. R.; Geraldes, L. R.; Zanotto, L. N.; Moreira, K. G.; Martins, O. P.; Piva, H. L.; Felipe, M. S. S.; Amaral, A. C.; Bocca, A. L.; Tedesco, A. C.; Mortari, M. R. *Sci. Rep.* **2021**, *11*, 15185.
(36) Zorkina, Y.; Abramova, O.; Ushakova, V.; Morozova, A.; Zubkov, E.; Valikhov, M.; Melnikov, P.; Majouga, A.; Chekhonin, V. Nano Carrier Drug Delivery Systems for the Treatment of Neuropsychiatric Disorders: Advantages and Limitations. *Molecules* **2020**, *25*, 5294.
(37) Yarjanli, Z.; Ghaedi, K.; Esmaeili, A.; Rahgozar, S.; Zarrabi, A. Iron oxide nanoparticles may damage to the neural tissue through iron accumulation, oxidative stress, and protein aggregation. *BMC Neurosci.* **2017**, *26*, 51.
(38) Lieberman, M.; Marks, A.; Peet, A.; *Marks' Basic Medical Biochemistry: A clinical approach*; (4th edition), 2013, ISBN-9781608315727.
(39) Bell, D. R. *Medical physiology: principles for clinical medicine*; Lippincott Williams & Wilkins: Philadelphia, p 312., (3rd ed.), 2009, ISBN − 9780787168528.
(40) Khurana *Medical physiology, Essentials of medical physiology*; 2009; p. 460, ISBN- 9788131215661.
(41) Buckley, E. *Venomous Animals and Their Venoms: Venomous Vertebrates*; 2013,p 478, ISBN − 9781483262888.
(42) *Animal Physiology: Adaptation and Environment* (5th ed.), Cambridge University press, 1997; p.510, ISBNN − 9781107268500.
(43) *'Epinephrine' the American Society of health-system pharmacists*; 2015.
(44) Kirshner, N.; Goodall, M. Formation of Adrenaline and Noradrenaline. *Biochim. Biophys. Acta* **1957**, *24* (3), 658−659.
(45) Yadav, T.; Sahu, R. K.; Mukherjee, V. Molecular modeling and spectroscopic investigation of a neurotransmitter: Epinephrine. *J. Mol. Struct.* **2019**, *1176*, 94−109.
(46) Frisch, M. J.; Trucks, G. W.; Schlegel, H. B.; Scuseria, G. E.; Robb, M. A.; Cheeseman, J. R.; Scalmani, G.; Barone, V.; Mennucci, B.; Petersson, G. A.; Nakatsuji, H.; Caricato, M.; Li, X.; Hratchian, H. P.; Izmaylov, A. F.; Bloino, J.; Zheng, G.; Sonnenberg, J. L.; Hada, M.; Ehara, M.; Toyota, K.; Fukuda, R.; Hasegawa, J.; Ishida, M.; Nakajima, T.; Honda, Y.; Kitao, O.; Nakai, H.; Vreven, T.; Montgomery, Jr., J. A.; Peralta, J. E.; Ogliaro, F.; Bearpark, M.; Heyd, J. J.; Brothers, E.; Kudin, K. N.; Staroverov, V. N.; Keith, T.; Kobayashi, R.; Normand, J.; Raghavachari, K.; Rendell, A.; Burant, J. C.; Iyengar, S. S.; Tomasi, J.; Cossi, M.; Rega, N.; Millam, J. M.; Klene, M.; Knox, J. E.; Cross, J. B.; Bakken, V.; Adamo, C.; Jaramillo, J.; Gomperts, R.; Stratmann, R. E.; Yazyev, O.; Austin, A. J.; Cammi, R.; Pomelli, C.; Ochterski, J. W.; Martin, R. L.; Morokuma, K.; Zakrzewski, V. G.; Voth, G. A.; Salvador, P.; Dannenberg, J. J.; Dapprich, S.; Daniels, A. D.; Farkas, O.; Foresman, J. B.; Ortiz, J. V.; Cioslowski, J.; Fox, D. J. *Gaussian 09, Revision E.01*; GAUSSIAN 09, Inc.: Wallingford CT, 2013.
(47) Darmandeh, H.; Löffler, J.; Tzouras, N. V.; Dereli, B.; Scherpf, T.; Feichtner, K.; Vanden Broeck, S.; Van Hecke, K.; Saab, M.; Cazin, C. S. J.; Cavallo, L.; Nolan, S. P.; Gessner, V. H. Au···H-C Hydrogen Bonds as Design Principle in Gold(I) Catalysis. *Angew. Chem., Int. Ed.* **2021**, *60*, 21014−21024.
(48) Vishwkarma, A. K.; Yadav, T.; Pathak, A.; Brahmachari, G. Interaction of a synthetic bio-relevant drug-molecule with C_{24} and $B_{12}N_{12}$ fullerene: A first-principles quantum chemical investigation. *Diam. and Relat. Mater.* **2023**, *132*, No. 109639.
(49) Rakib Hossain, M.; Mehade Hasan, M.; Ud Daula Shamim, S.; Ferdous, T.; Abul Hossain, M.; Ahmed, F. First-principles study of the adsorption of chlormethine anticancer drug on C24, B12N12 and B12C6N6 nanocages. *Compt. Theor. Chem.* **2021**, *1197*, No. 113156.
(50) Rad, A. S.; Aghaei, S. M.; Aali, E.; Peyravi, M. Study on the electronic structure of Cr- and Ni-doped fullerenes upon adsorption of adenine: A comprehensive DFT calculation. *Diam. Relat. Mater.* **2017**, *77*, 116−121.
(51) Ahmadi Peyghan, A.; Hadipour, N. L.; Bagheri, Z. Effects of Al Doping and Double-Antisite Defect on the Adsorption of HCN on a BC2N Nanotube: Density Functional Theory Studies. *J. Phys. Chem. C* **2013**, *117*, 2427−2432.
(52) Nhat, P. V.; Si, N. T.; Tram, N. T. T.; Duong, L. V.; Nguyen, M. T. Elucidating the binding mechanism of thione-containing mercaptopurine and thioguanine drugs to small gold clusters. *J. Comput. Chem.* **2020**, No. 41, 1748−1758.
(53) O'Boyle, N. M.; Tenderholt, A. L.; Langner, K. M. cclib: A library for package-independent computational chemistry algorithms. *J. Comput. Chem.* **2008**, *29*, 839−845.
(54) Tomasi, J.; Mennucci, B.; Cammi, R. Quantum Mechanical Continuum Solvation Models. *Chem. Rev.* **2005**, *105*, 2999−3093.
(55) Kaviani, S.; Shahab, S.; Sheikhi, M.; Potkin, V.; Zhou, H. A DFT study of Se-decorated B12N12 nanocluster as a possible drug delivery system for ciclopirox. *Compt and Theor. Chem.* **2021**, *1201*, No. 113246.
(56) Knozinger, H.; Kochloefl, K. Heterogeneous Catalysis and Solid Catalysts. *Ullmann's Encyclopedia of Industrial Chemistry*; Wiley-VCH Verlag:, Weinheim, Germany, 2005, 1−110.
(57) Ordaz, J. C.; Anota, E. C.; Villanueva, M. S.; Castro, M. Possibility of a magnetic [BN fullerene: B6 cluster]− nanocomposite as a vehicle for the delivery of dapsone. *New J. Chem.* **2017**, *41*, 8045−8805.
(58) Yadav, T.; Shakerzadeh, E.; Vishwkarma, A. K.; Singh, P. K.; Pathak, A.; Chakroborty, S.; Pandey, F. P.; Moharana, S.; Kumar, R. Histamine sensing by Boron and Silicon doped C60 Fullerenes: A first principles investigation. *Diam. Relat.Mater.* **2023**, *140*, No. 110471.
(59) Dhaka, K.; Trivedi, R.; Bandyopadhyay, D. Electronic structure and stabilities of Ni-doped germanium nanoclusters: a density functional modeling study. *J. Mol. Model* **2013**, *19*, 1473−1488.
(60) Bandyopadhyay, D. Electronic structure and stability of anionic AuGen (n = 1−20) clusters and assemblies: a density functional modeling. *Structural Chemistry* **2019**, *30*, 955−963.
(61) Yadav, T.; Mukherjee, V. Optimization of synephrine and its vibrational and electronic structures. *Vib. Spect.* **2020**, *106*, 102089.
(62) Bandyopadhyay, D.; Sen, P. Density Functional Investigation of Structure and Stability of Gen and GenNi (n = 1−20) Clusters: Validity of the Electron Counting Rule. *J. Phys. Chem. A* **2010**, *114* (4), 1835−1842.
(63) Yadav, T.; Brahmachari, G.; Karmakar, I.; Yadav, P.; Agarwal, A.; Mukherjee, V.; Pathak, A.; Dubey, N. K. Synthesis, structural and vibrational spectroscopic investigation of molecules: N-n-butyl, S-2-nitro-1-phenylethyl dithiocarbamate and N-n-butyl, S-2-nitro-1-(4-flurophenyl)ethyl dithiocarbamate. *Vib. Spect.* **2020**, *111*, No. 103151.

https://doi.org/10.1021/acsomega.3c06382
ACS Omega 2024, 9, 3373−3383